

Group-scale intrinsic galaxy alignments in the Illustris-TNG and MassiveBlack-II simulations

Ananth Tenneti^{1*}, Thomas D. Kitching¹, Benjamin Joachimi², Tiziana Di Matteo³

¹*Mullard Space Science Laboratory, University College London, Holmbury St Mary, Dorking, Surrey RH5 6NT, UK*

²*Department of Physics and Astronomy, University College London, Gower Street, London WC1E 6BT, UK*

³*McWilliams Center for Cosmology, Dept. of Physics, Carnegie Mellon University, Pittsburgh PA 15213, USA*

21 December 2024

ABSTRACT

We study the alignments of satellite galaxies, and their anisotropic distribution, with respect to location and orientation of their host central galaxy in MassiveBlack-II and IllustrisTNG simulations. We find that: the shape of the satellite system in halos of mass ($> 10^{13} h^{-1} M_{\odot}$) is well aligned with the shape of the central galaxy at $z = 0.06$ with the mean alignment between the major axes being $\sim \Delta\theta = 12^{\circ}$ when compared to a uniform random distribution; that satellite galaxies tend to be anisotropically distributed along the major axis of the central galaxy with a stronger alignment in halos of higher mass or luminosity; and that the satellite distribution is more anisotropic for central galaxies with lower star formation rate, which are spheroidal, and for red central galaxies. Radially we find that satellites tend to be distributed along the major axis of the shape of the stellar component of central galaxies at smaller scales and the dark matter component on larger scales. We find that the dependence of satellite anisotropy on central galaxy properties and the radial distance is similar in both the simulations with a larger amplitude in MassiveBlack-II. The orientation of satellite galaxies tends to point toward the location of the central galaxy at small scales and this correlation decreases with increasing distance, and the amplitude of satellite alignment is higher in high mass halos. However, the projected ellipticities do not exhibit a scale-dependent radial alignment, as has been seen in some observational measurements.

Key words: cosmology: theory – methods: numerical – hydrodynamics – gravitational lensing: weak – galaxies: star formation

1 INTRODUCTION

The intrinsic alignment (IA) of galaxies is a significant systematic in the science analysis of upcoming weak lensing surveys (Kirk et al. 2012; Krause et al. 2016). IAs are also of interest as a probe of the physics of galaxy formation and evolution. The next generation ground and space-based telescope surveys such as the Large Synoptic Survey Telescope¹ (LSST; LSST Science Collaboration et al. 2009), *Euclid*² (Laureijs et al. 2011) and Wide-Field Infrared Survey Telescope³ (WFIRST; Spergel et al. 2015) aim to employ weak lensing to constrain cosmological parameters to sub-percent level precision. However, it is well known that IAs are a contaminant in weak lensing measurements, and not taking the

effect of IA into account can lead to a bias in the constraints of cosmological parameters such as the dark energy equation of state of up to $\sim 70\%$ (Krause et al. 2016). However, the effect of IAs can be mitigated by marginalizing over nuisance parameters in analytical models of IA (Joachimi & Bridle 2010; Blazek et al. 2012). The most straightforward way in which IAs have been modelled analytically is through the linear alignment model (Catelan et al. 2001; Hirata & Seljak 2004), and extensions of it to non-linear scales (Bridle & King 2007; Blazek et al. 2015). However, on smaller scales this modelling becomes less physically motivated and so instead halo model prescriptions have been proposed to model IAs. A small scale halo model of IA was developed by Schneider & Bridle (2010). This model assumes that the satellite galaxies are distributed symmetrically around the central galaxy and are oriented towards the central. In this paper, we test these assumptions on small scale galaxy alignments in the MassiveBlack-II (Khandai et al. 2015)

* E-mail: a.tenneti@ucl.ac.uk

¹ <https://www.lsst.org/lsst/>

² <http://sci.esa.int/euclid/>, <https://www.euclid-ec.org/>

³ <https://wfirst.gsfc.nasa.gov/>

and IllustrisTNG (Nelson et al. 2019; Pillepich et al. 2018b; Springel et al. 2018; Nelson et al. 2018; Naiman et al. 2018; Marinacci et al. 2018) cosmological hydrodynamic simulations. In particular, we study the distribution and orientation of satellite galaxies with respect to the location and orientation of their host central galaxy.

Cosmological simulations of galaxy formation have emerged as a useful tool to study IA and baryonic effects on weak lensing. For example IAs have been studied in simulations such as MassiveBlack-II (Khandai et al. 2015), Horizon-AGN (Dubois et al. 2014), EAGLE (Schaye et al. 2015) and Illustris (Vogelsberger et al. 2014b,a; Genel et al. 2014). The measurements of IA correlation functions from simulations have been found to be in good agreement with observations and broadly in agreement with each other, in particular results as a function of properties such as galaxy mass, luminosity and also the radial scaling of the alignment signal (Tenneti et al. 2015; Velliscig et al. 2015; Chisari et al. 2015; Hilbert et al. 2017). It has to be noted though that some differences pertaining to tangential alignment of disk galaxies have been identified across simulations (Chisari et al. 2015; Tenneti et al. 2016). Samuroff et al. (2019) used the MassiveBlack-II and Illustris simulations to consider the impact of the assumption of the spherically symmetric distribution of satellite galaxies used in the halo model of Schneider & Bridle (2010) for small scale intrinsic alignments modelling. Samuroff et al. (2019) found that the anisotropic satellite distribution seen in the simulations leads to biases on the cosmological parameter constraints from weak lensing when alignments are modelled using the halo model. Shao et al. (2016) used the EAGLE simulation to study the alignment of the central galaxy with the shape traced by the satellites in the halo. Welker et al. (2015) studied the distribution of satellites in the plane of central galaxy and with respect to filaments in the Horizon-AGN simulation. Galaxy alignments in groups have also been studied through observations. Huang et al. (2016, 2018) used the redMaPPer cluster catalog data to study the central galaxy alignment with the satellite distribution and the radial alignment of satellite galaxies with respect to groups. More recently, Georgiou et al. (2019) used the GAMA+KiDS data to study the scale dependence of satellite alignments with respect to the central galaxy. In this paper, we measure the alignments of the shape of central galaxy with the shape of the satellite system to compare against earlier simulation results. Measurements in MassiveBlack-II and IllustrisTNG simulations will also help to explore any differences in satellite galaxy alignments due to baryonic feedback models. We also present the scale dependent radial alignments of satellite shapes for comparison with the observational measurements of galaxy alignments in groups (Georgiou et al. 2019).

The rest of the paper is organized as follows. In Section 2, we provide the details of MassiveBlack-II and Illustris simulation along with the methods adopted in the paper. In Section 3, we present the results on the alignments of the central galaxy shape with the shape of the satellite system and the distribution of satellite galaxies along the central galaxy. We explore the dependence on various galaxy properties such as mass, luminosity, color and morphological type. In this section, we also present the small-scale galaxy alignment correlation functions in 3D, as well as projected

correlation functions for comparison with observations. Finally, we present conclusions in Section 4.

2 METHODS

In this paper, we analyze the anisotropic distribution of satellites in the Illustris-TNG and MassiveBlack-II simulations. The details of the simulations are described below.

2.1 Simulations: Illustris-TNG and MassiveBlack-II

MassiveBlack-II (MB-II) is a state-of-the-art high resolution, large volume, cosmological hydrodynamic simulation of structure formation. This simulation has been performed with P-GADGET, which is a hybrid version of the parallel code, GADGET2 (Springel et al. 2005) upgraded to run on Petaflop scale supercomputers. In addition to gravity and smoothed-particle hydrodynamics (SPH), the P-GADGET code also includes the physics of multiphase ISM model with star formation (Springel & Hernquist 2003), black hole accretion and feedback (Springel et al. 2005; Di Matteo et al. 2012). Radiative cooling and heating processes are included (as in Katz et al. 1996), as is photoheating due to an imposed ionizing UV background. The details of this simulation can be found in Khandai et al. (2015).

MB-II contains $N_{\text{part}} = 2 \times 1792^3$ dark matter and gas particles in a cubic periodic box of length $100h^{-1}h^{-1}\text{Mpc}$ on a side, with a gravitational smoothing length $\epsilon = 1.85h^{-1}\text{kpc}$ in comoving units. A single dark matter particle has a mass $m_{\text{DM}} = 1.1 \times 10^7 h^{-1}M_{\odot}$ and the initial mass of a gas particle is $m_{\text{gas}} = 2.2 \times 10^6 h^{-1}M_{\odot}$, with the mass of each star particle being $m_{\text{star}} = 1.1 \times 10^6 h^{-1}M_{\odot}$. The cosmological parameters used in the simulation are according to WMAP7 (Komatsu et al. 2011).

The IllustrisTNG simulation is performed with the AREPO TREEPM moving-mesh code (Springel 2010) in a box of volume $(75h^{-1}\text{Mpc})^3$. The galaxy formation physics includes subgrid-model for star formation and associated supernova feedback, black hole accretion and feedback, stellar wind feedback, primordial and metal-line radiative cooling and magnetic fields. A detailed description of the models can be found in Weinberger et al. (2017) and Pillepich et al. (2018a). The simulation follows 2×1820^3 dark matter particles and gas particles with a gravitational smoothing length of 1.4 comoving kpc for the dark matter particles. The mass of each dark matter particle is $5.1 \times 10^6 h^{-1}M_{\odot}$ and the initial mass of gas particle is $9.4 \times 10^5 h^{-1}M_{\odot}$. The cosmological parameters are based on Planck (Planck Collaboration et al. 2016).

2.2 Shape calculation

The shapes of the stellar matter component in subhalos are modeled as ellipsoids in three dimensions using the eigenvalues and eigenvectors of the reduced inertia tensor.

$$\tilde{I}_{ij} = \frac{\sum_n m_n \frac{x_{n,i} x_{n,j}}{r_n^2}}{\sum_n m_n}, \quad (1)$$

where the summation is over particles indexed by n , and

$$r_n^2 = \sum_i x_{n,i}^2. \quad (2)$$

Here, m_n is the mass of the n^{th} particle and $x_{n,i}$ is the position co-ordinate of the n^{th} particle for $0 \leq i \leq 2$ in 3D. We note that the effect of weighting instead with a star particle's luminosity instead of mass is investigated in Tenneti et al. (2015) and found to have negligible impact on the derived shape distributions. Similar to earlier studies, we only choose galaxies with a minimum of 1000 dark matter and star particles for resolved shapes. The reduced inertia tensor gives more weight to particles that are closer to the center of the subhalo in question, which reduces the influence of loosely bound particles present in the outer regions of the subhalo. The shapes are determined iteratively using the reduced inertia tensor as detailed in Tenneti et al. (2015). In 3D, the eigenvectors of the inertia tensor are $\hat{e}_a, \hat{e}_b, \hat{e}_c$ with corresponding eigenvalues $\lambda_a > \lambda_b > \lambda_c$. The eigenvectors represent the principal axes of the ellipsoid, with the half-lengths of the principal axes (a, b, c) given by $(a, b, c) = (\sqrt{\lambda_a}, \sqrt{\lambda_b}, \sqrt{\lambda_c})$. The 3D axis ratios are

$$q = \frac{b}{a}, \quad s = \frac{c}{a}. \quad (3)$$

The projected shapes are calculated by projecting the positions of the particles onto the XY plane of the simulation box and modeling the shapes as ellipses. In 2D, the eigenvectors are \hat{e}'_a, \hat{e}'_b with corresponding eigenvalues $\lambda'_a > \lambda'_b$. The lengths of the semi-major and semi-minor axes are $a' = \sqrt{\lambda'_a}$ and $b' = \sqrt{\lambda'_b}$ with axis ratio $q_{2D} = b'/a'$.

2.3 Shape of the satellite system

We define the shape of the satellite system for a given halo as the shape traced by the positions of the satellite galaxies of the halo. The shape is determined by the mass weighted inertia tensor given by

$$I_{ij}^{\text{Sat}} = \frac{\sum_n m_n x_{n,i} x_{n,j}}{\sum_n m_n}, \quad (4)$$

where m_n is mass of the n^{th} subhalo and $x_{n,i}$ refers to the satellite position. Similar to the shape calculation method, the eigenvector decomposition of the inertia tensor will give the major axes of the shape traced by the satellite system. This definition is similar to the one adopted by Shao et al. (2016). The alignment of the shape of the satellite system with that of the central galaxy will help us understand the distribution of satellite galaxies in the halo. A stronger alignment will indicate a tendency for the satellite galaxies to be distributed along the major axis of the central galaxy.

3 RESULTS

In this section, we discuss our findings on the anisotropic distribution of the satellite galaxies with the orientation of central galaxy as well as the orientation of satellite galaxies with respect to the central in MassiveBlack-II and IllustrisTNG simulations.

3.1 Alignment of central galaxy shape with shape of satellite system

We first explore the alignment between the shape of the dark matter and stellar matter component of the central galaxy with the shape traced by the satellite system within the halo. The shape of the satellite system is obtained using the positions of satellite galaxies within the halo as described in Section 2.3. Here, we consider only halos with masses above $10^{13} h^{-1} M_\odot$ to allow for sufficient satellite galaxies at $z = 0.06$. In Figure 1, we plot the distribution of the alignment angles between the shape of the satellite system and the shape of the central galaxy, determined by the dark matter and stellar matter component of the galaxy. The 3D alignments are shown in the *Top panel* of the figure, while the *Bottom panel* shows the projected alignments. In the left hand side of the top panel, we show the normalized distribution of the 3D alignments. We can see that the satellite system tends to be aligned with the shape of the central galaxy, when compared with that of a random distribution. Clearly, the satellite system has a higher degree of alignment with the dark matter component. This implies that on average, the satellite galaxies tend to be anisotropically distributed along the major axis of the shape of the central galaxy in comparison to the shape of stellar component. The mean alignment angles are $33.08^\circ \pm 1.25^\circ$ and $44.19^\circ \pm 1.28^\circ$ respectively for the shape of dark matter component and stellar component respectively in Massive-Black II. In Illustris-TNG, the mean misalignment angles are $33.78^\circ \pm 1.85^\circ$ and $45.95^\circ \pm 1.89^\circ$.

Observationally, Huang et al. (2016) studied the projected alignments of the central galaxy with the shape traced by the satellites in redMaPPer clusters and found a mean misalignment angle of $\sim 35^\circ$ and the alignment is found to be stronger in central galaxies of higher luminosity. Here, we do not investigate the mass dependence due to fewer satellites in halos of lower mass for resolving shapes. Further, it is found that satellites close to the central galaxies are more anisotropically distributed along the central major axis. We discuss the radial dependence of the anisotropic distribution in the subsections below. The right panels of Figure 1 show the cumulative distribution of the cosine of the alignment angle between the orientations of the shapes. We can clearly see that the degree of alignment is significant when compared to a random uniform distribution. Comparing the distributions in MassiveBlack-II and Illustris-TNG, we can see that the alignment trend is very similar and the cumulative distributions are consistent with each other. In the bottom panel of Figure 1, we similarly show the alignment distributions in 2D. The alignments are much stronger when compared with the 3D alignments. Further, the alignments are similar for both MB-II and Illustris-TNG, as in the case of 3D alignments.

In order to understand the mass dependent trend of the satellite distribution, we plot the histogram of orientation between the shape of the stellar component of the central galaxy and the location of satellite galaxies in Figure 2 for halos of mass range, $10^{11-12} h^{-1} M_\odot$, $10^{12-13} h^{-1} M_\odot$ and $10^{13-15} h^{-1} M_\odot$. From the figure, we can observe a mass dependent trend in the distribution of satellites in the MassiveBlack-II simulation. The satellite galaxies tend to be distributed along the major axis of the central galaxy with a higher degree of alignment in high mass halos. From previ-

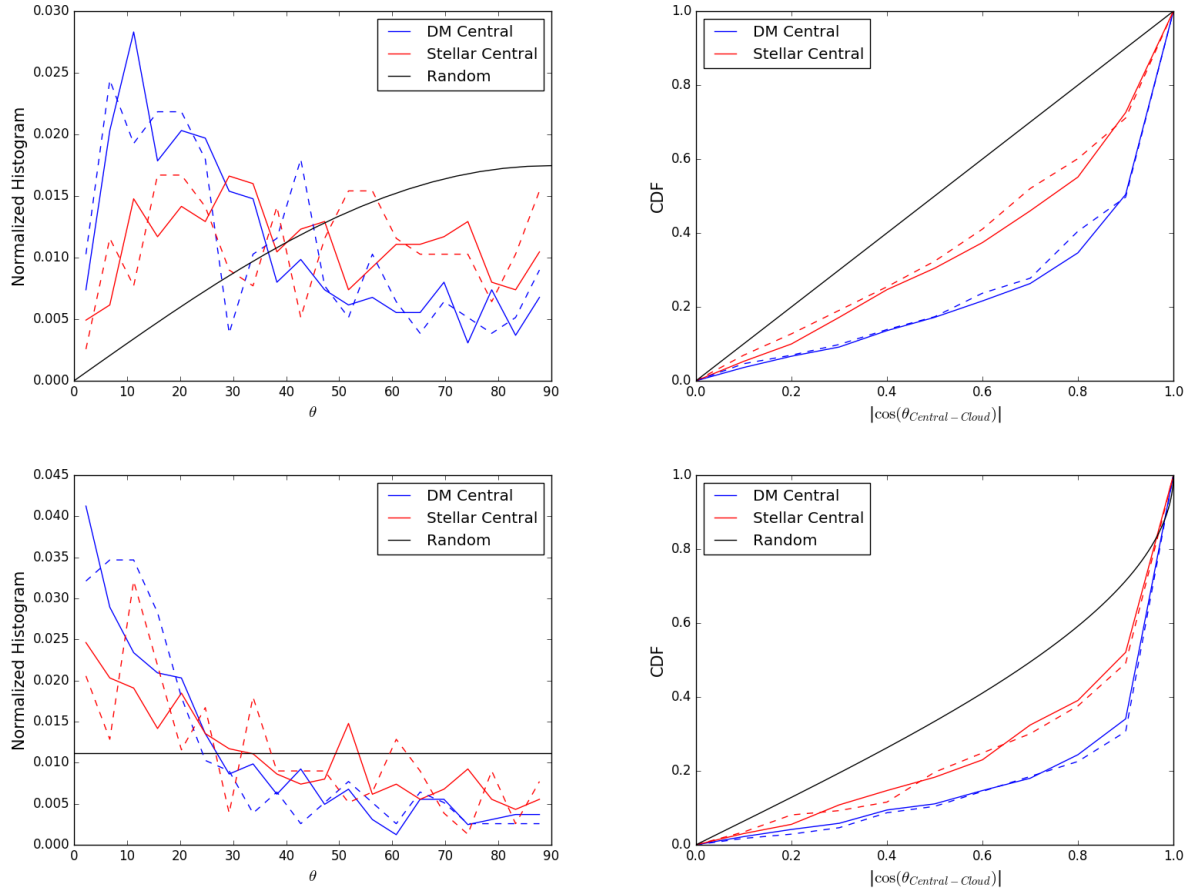


Figure 1. Alignment of the shape of the dark matter and stellar matter component of the central galaxies of halo mass ($> 10^{13} h^{-1} M_{\odot}$) with the shape of the satellite system. *Top panel:* 3D alignments, *Bottom panel:* 2D alignments. The normalized distribution of alignment angles is shown in the *Left column*, while the *Right column* shows the cumulative distribution of the cosine of the alignment angles. The solid lines show the distributions for the MassiveBlack-II simulation and the dashed lines represent the Illustris-TNG simulation.

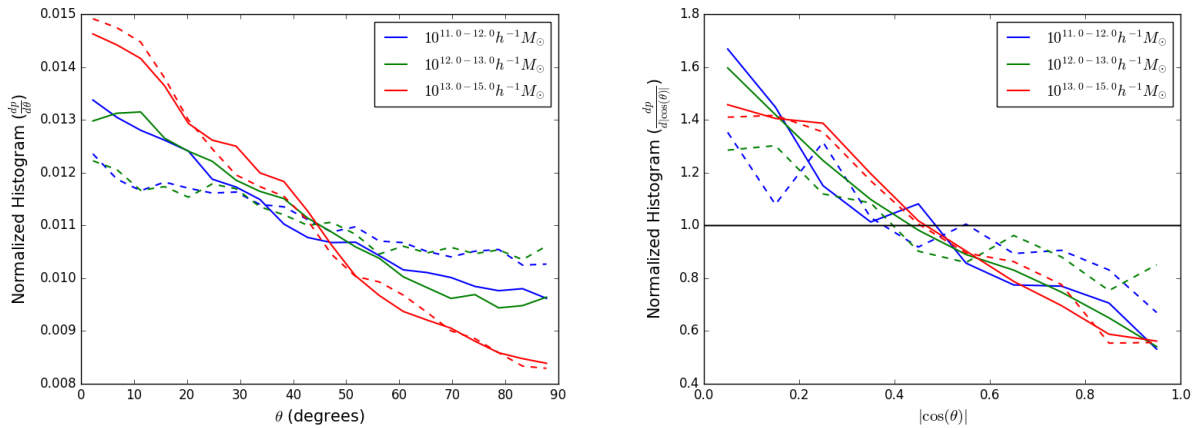


Figure 2. Normalized distribution of the alignment angles between the 2D shape of the stellar matter component of the central galaxy and the location of satellite galaxies in MassiveBlack-II and Illustris-TNG (*Left*). The (*Right*) panel shows the distribution of the cosine of the angle between the minor axis of the stellar shape in 3D and the location of the satellite galaxies (*Right*). The histograms are shown for halos of mass, $10^{11-12} h^{-1} M_{\odot}$, $10^{12-13} h^{-1} M_{\odot}$ and $10^{13-15} h^{-1} M_{\odot}$. The solid lines show the distributions for the MassiveBlack-II simulation and the dashed lines represent the Illustris-TNG simulation.

ous studies based on MassiveBlack-II (Tenneti et al. 2015), it is known that the stellar shape is more misaligned with the shape of dark matter halo in halos of lower mass. Since, the satellite system is more aligned with the shape of dark matter halo as discussed earlier, we expect the satellite distribution to be more anisotropic in high mass halos, due to the larger alignment of the stellar shape. The trend is similar in the Illustris-TNG simulation as well. From the figure, we can also observe that the satellite distribution is more anisotropic in the MassiveBlack-II simulation for the lower halo mass bins. In a previous study (Tenneti et al. 2016), the stellar component of galaxies in Illustris simulation is found to be more misaligned with the dark matter component when compared with the MassiveBlack-II simulation. These differences in galaxy alignments are likely due to the different baryonic feedback models adopted in the two simulations. Since the feedback model adopted in Illustris-TNG is more similar to that of the Illustris simulation, the stronger anisotropic distribution of satellite galaxies in MassiveBlack-II is consistent with Tenneti et al. (2016) results. Welker et al. (2015) found that the satellite galaxies tend to be distributed along the plane of the central galaxy perpendicular to the direction of the minor axis. We similarly plot the histogram of the orientation of the minor axis of the central shape with the location of the satellite positions. As seen from the histogram of the cosine of the angle in the right panel of Figure 2, we see that there is an excess probability for the cosine of the angle to be 0, which indicates that the satellites are distributed along the plane of the galaxy. We do not find a significant mass dependent trend here.

3.2 Distribution of satellite galaxies with orientation of central galaxy: dependence on central galaxy properties

Here, we consider the dependence of the anisotropic distribution of satellite galaxies on properties of the central galaxy. In Figure 3, we plot the distribution of satellite galaxies based on the properties, such as luminosity, morphological type, color and star formation rate. Here, the luminosity of the galaxy is based on the SDSS r -band absolute magnitude in the rest frame (M_r). We define three luminosity bins, with $-26.3 \leq M_r < -23$, $-23 \leq M_r < -20$ and $-20 \leq M_r < -17$. The galaxy colors ($g - r$) are defined as the difference of the rest-frame absolute magnitudes in the SDSS g -band and SDSS r -band. In this study, we chose the median of the $g - r$ colors to split the galaxy sample into red and blue galaxies. The galaxies with low and high SFR are similarly defined based on the median of the galaxy star formation rates in the sample.

The classification of galaxies in MassiveBlack-II into disks and spheroids is done based on a dynamical bulge-disc decomposition (as discussed in Tenneti et al. 2016) where all the galaxies with bulge-to-total ratio less than 0.7 are classified as disks. The disk galaxies in Illustris-TNG are similarly defined.

We can see that the luminosity trend is similar to that of the halo mass, with more satellites distributed along the major axis of galaxies with larger luminosity. Shao et al. (2016) found a dependence in the alignment of satellite distribution based on whether the central galaxy is disc or spheroid. To compare with their results, we similarly split the central

galaxies in our sample into discs and spheroids. However, we do not find a significant difference in the satellite distribution in MassiveBlack-II. As seen from the figure, the distribution of satellites is similar for both discs and spheroid galaxies. However, we find a color-dependent trend in the satellite distribution, with the red central galaxies showing a larger anisotropic distribution of the satellites along their major axes. The Illustris-TNG simulation results show a stronger tendency for the satellites in red central galaxy and spheroid galaxies to be distributed along the major axis. By comparing the satellite distribution in central galaxies split based on their star formation rate (SFR), we find a slightly higher tendency for the satellites in centrals of low SFR to be distributed along the major axis of centrals in both MassiveBlack-II and Illustris-TNG. We also find that the coplanar distribution of the satellite galaxies is stronger in spheroids, red centrals and galaxies with low SFR.

3.3 Small-scale alignments : Correlation functions and comparison with observational measurements

In this Section, we consider the radial dependence of the correlation of a central galaxy shape with the location of satellites and the shape of the satellite galaxy with the location of its host halo. Accordingly, we calculated the small-scale shape-density correlation functions (within the halo, corresponding to the 1-halo term) in 3D. We also consider projected radial ellipticities of the galaxy shapes for comparison with observational measurements.

In order to understand the radial dependence of the distribution of satellite galaxies along the major axis of the central galaxy, we consider the Ellipticity-Density (ED) correlation function for the shape of the stellar component of central galaxies in Figure 4. For a galaxy with orientation of major axis, $\hat{e}(\mathbf{r})$ and density tracers located at a distance r in the direction of the unit vector, \hat{r} , the ED correlation is given by the mean,

$$\omega(r) = \langle |e(\hat{\mathbf{r}}) \cdot \hat{r}|^2 \rangle - \frac{1}{3}. \quad (5)$$

Here the shape of the central galaxy is cross-correlated with the satellite positions only within the halo corresponding to the central galaxy.

The left panel of Figure 4 shows the ED correlation function in the MassiveBlack-II simulation, while the right panel corresponds to the results in IllustrisTNG simulation. The correlation function is plotted for the halos within the mass bins, $10^{11-12} h^{-1} M_\odot$, $10^{12-13} h^{-1} M_\odot$, and $10^{13-15} h^{-1} M_\odot$ by cross-correlating the shape of a central galaxy with the location of the satellite galaxies inside the halo. At very small scales ($< 0.1 h^{-1} \text{Mpc}$), we can see that the correlation function shows a decreasing trend with distance from the galaxy center. This indicates that the satellite galaxies close to the central galaxy are distributed along the major axis of the stellar shape and tend to be more symmetrically distributed as the distance from the central galaxy increases. However at larger distances close to the halo boundary ($\sim 0.1 - 1 h^{-1} \text{Mpc}$), we can clearly see an increase in the correlation function. This is because at larger distances, the satellites tend to be more anisotropically dis-

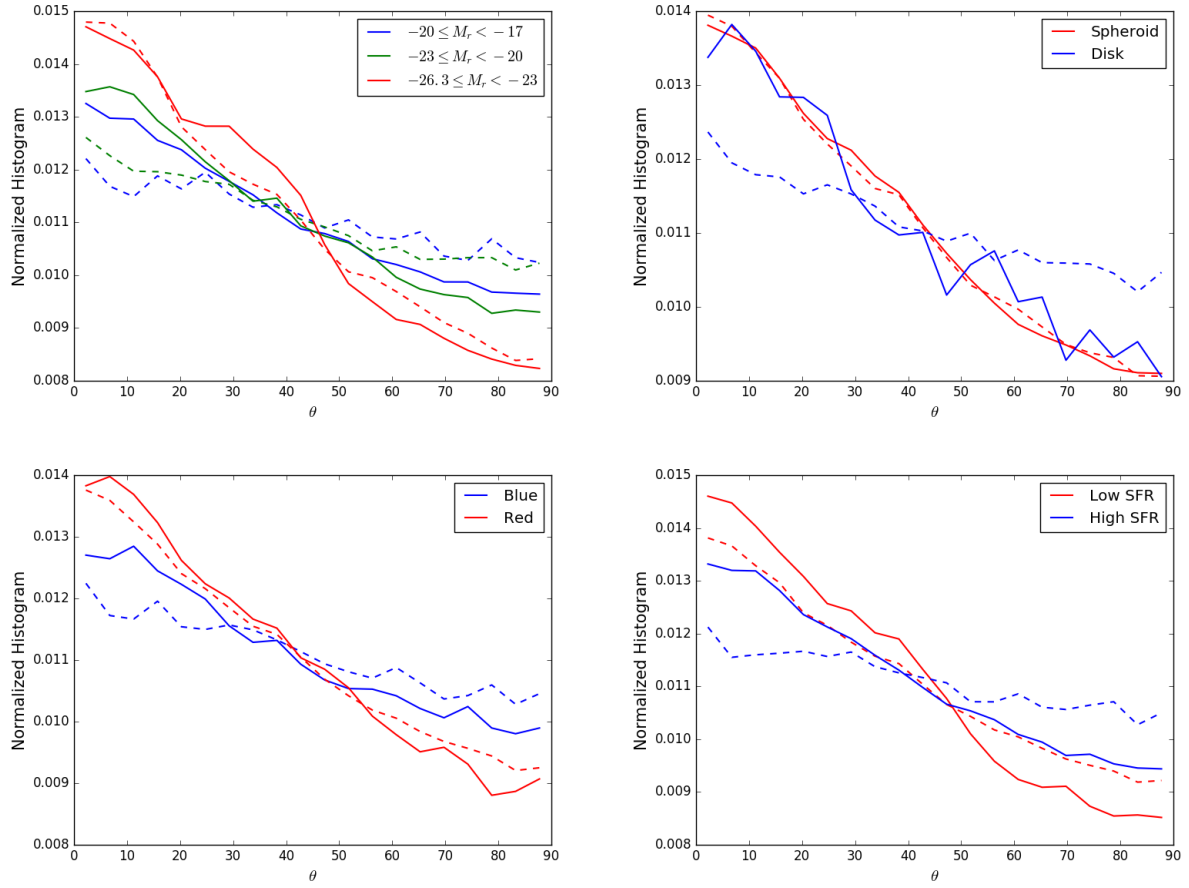


Figure 3. Normalized distribution of the alignment angles between the 2D shape of the stellar matter component of the central galaxy and the location of satellite galaxies in MassiveBlack-II and Illustris-TNG simulations based on the central galaxy properties: Luminosity(*top left*), morphology(*top right*), Color(*bottom left*), star formation rate(*bottom right*). Here, the solid lines show the distributions for the MassiveBlack-II simulation and the dashed lines represent the Illustris-TNG simulation.

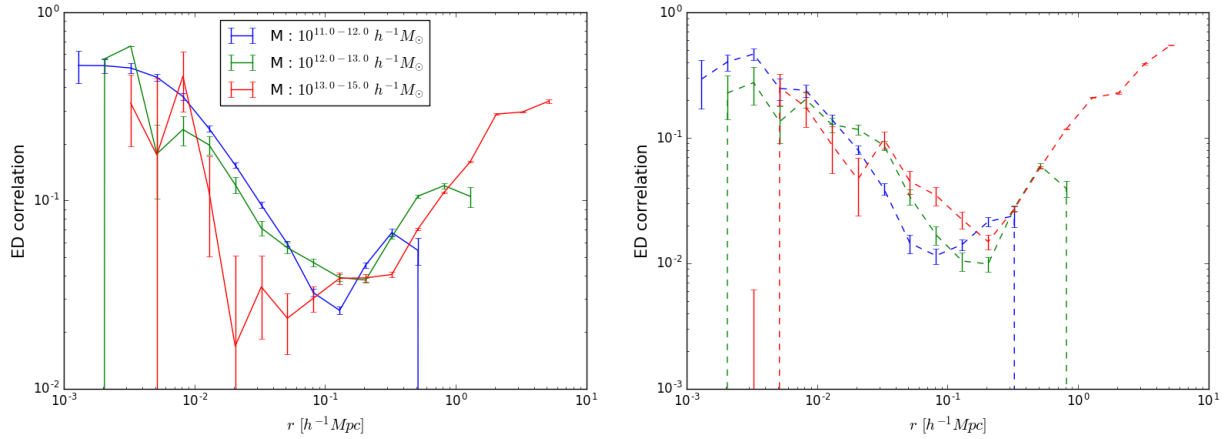


Figure 4. Ellipticity-direction (ED) correlation function of the 3D shape of the central galaxy with the location of the satellite galaxies within the given halo in MassiveBlack-II (*Left*) and Illustris-TNG (*Right*) simulations. The correlation functions are plotted in halos of mass bins, $10^{11-12} h^{-1} M_{\odot}$, $10^{12-13} h^{-1} M_{\odot}$ and $10^{13-15} h^{-1} M_{\odot}$ at redshift, $z = 0.06$. Here, we cross-correlate with the positions of all subhalos in the halo without a mass threshold. The non-negligible signal on a kpc scale is due to density peaks identified as subhalos. If we include a mass threshold in the density sample (satellite galaxies), we do not see a signal below $\sim 5 h^{-1} \text{kpc}$.

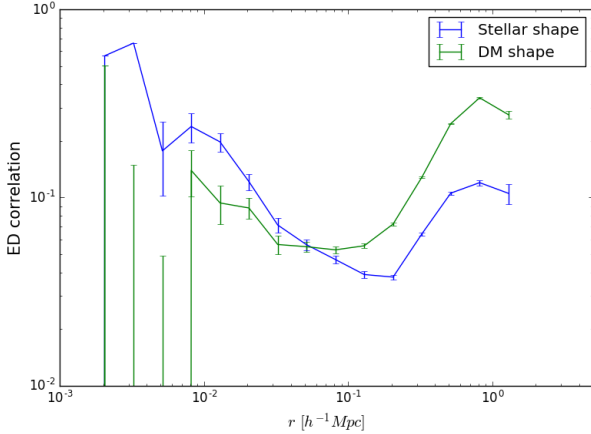


Figure 5. ED correlation for the shape of the dark matter and stellar component of the central galaxies in the MassiveBlack-II simulation with the density distribution traced by the positions of satellites within the corresponding halo. The correlation function is for the halos of mass, $10^{12-13} h^{-1} M_{\odot}$ at $z = 0.06$.

tributed along the major axis of the shape of the dark matter component of the galaxy with increasing distance. Since, the stellar shape is in turn correlated with the shape of the dark matter component, we also see a similar radial dependence of the distribution of the satellites w.r.t central galaxy on these scales (with smaller amplitude).

This is further illustrated in Figure 5, where the shape of the dark matter and stellar matter component of the galaxy is correlated with the location of satellites within the halo. At small scales, we can see that the amplitude of ED correlation function is higher for the shape of the stellar component while on large scales, it is larger for the shape of dark matter component. This indicates that on small scales, the satellites are distributed anisotropically along the major axis of the shape of the stellar component, while on large scales, they are distributed along the shape of the dark matter component. On intermediate scales, the satellite distribution tends to be uncorrelated with the shape of stellar component and hence, we observe a decreasing correlation function. The increase in correlation on large scales for the shape of stellar component is due to the correlation of the stellar shape with that of the dark matter component.

In Figure 6, we plot the ED correlation function with bins in r/r_{200} . This is to understand the dependence of the scale at which we find a transition of the signal from a decreasing trend to an increasing one on large scales. From the figure, we can see that there is no clear dependence of the transition scale on r_{200} . Instead, we find a clear mass dependence in the amplitude of the signal at small and large scales. The satellite distribution on smaller scales is more anisotropic along the major axis of the stellar shape in low mass halos as seen by the larger amplitude of ED correlation. However, as known from previous studies (Tenneti et al. 2015), the stellar shape in low mass galaxies is more misaligned with the shape of the dark matter subhalo, which leads to a lower correlation with satellite distribution on larger scales, which tends to be more correlated with the shape of the dark matter halo.

Comparing MassiveBlack-II and IllustrisTNG, we find

that the radial dependence (a decreasing correlation function, followed by an increase at scales closer to the limit of 1-halo regime) is similar in both simulations. We can also find a mass-dependence of the correlation functions with a higher amplitude at larger scales in halos of high-mass. There is also a mass-dependence in the scale at which the correlation function shows a tilt from the decreasing trend. However, at intermediate scales ($\sim 0.01 - 0.1 h^{-1} M_{\odot}$), we see that the correlation function is larger in low mass halos in the MassiveBlack-II simulation, while in the IllustrisTNG simulation, it is larger in high-mass halos. van Uitert et al. (2017) used the GAMA galaxy groups from weak lensing and found that the satellites in the outer halo trace the orientation of the dark matter subhalo. Similarly, consistent with our findings, the satellite distribution is found to be anisotropic with respect to the major axis of the BCG and the signal decreases with the distance from the center of the galaxy.

Similarly, we can also understand the radial dependence of the orientation of the shapes of the satellite galaxies with respect to the location of central galaxy. In the top panel of Figure 7, we plot the ED correlation of the shape of satellite galaxies in a halo of given mass with respect to the location of the central galaxy. From the figure, we can see that the correlation function decreases as the radial separation increases from the center of the halo. This indicates that the satellite shapes closer to the halo center have a stronger alignment towards the center. We can also see that the amplitude of alignment shows a mass dependent trend with a higher alignment in more massive halos.

Our results are consistent with observational measurements of Huang et al. (2018) in redMaPPer clusters. Huang et al. (2018) found that the alignments of satellite ellipticities with central galaxies decreases with the radial distance from central galaxy and is stronger in more luminous satellites. However, for Illustris-TNG we only find a decreasing trend with radial distance for the lowest mass bin ($10^{11-12} h^{-1} M_{\odot}$). For higher mass bins, the correlation is not significant and does not seem to exhibit a radial dependence. It is possible that this feature in Illustris-TNG simulation is due to baryonic feedback (Tenneti et al. 2017; Soussana et al. 2019). In order to understand this further, we also plot the alignments of satellites in Illustris simulation. These are shown by the dashed lines in the plot. Here, we can see that the radial dependence and halo mass dependence of satellite alignments is similar to what is observed in the MassiveBlack-II simulation. Since the numerical hydrodynamic scheme is similar in Illustris and Illustris-TNG, the differences can be attributed to baryonic feedback models.

We compare the measurements of the radial alignment of satellite galaxies in the simulation with recent observational measurements. Georgiou et al. (2019) measured the projected ellipticities of the shape of satellite galaxies with respect to the location of the central galaxy in GAMA+KiDS. Georgiou et al. (2019) measured the average ellipticity in radial bins and found that the average radial ellipticity decreases with radial distance. In order to compare with these measurements, we plot the mean of the radial

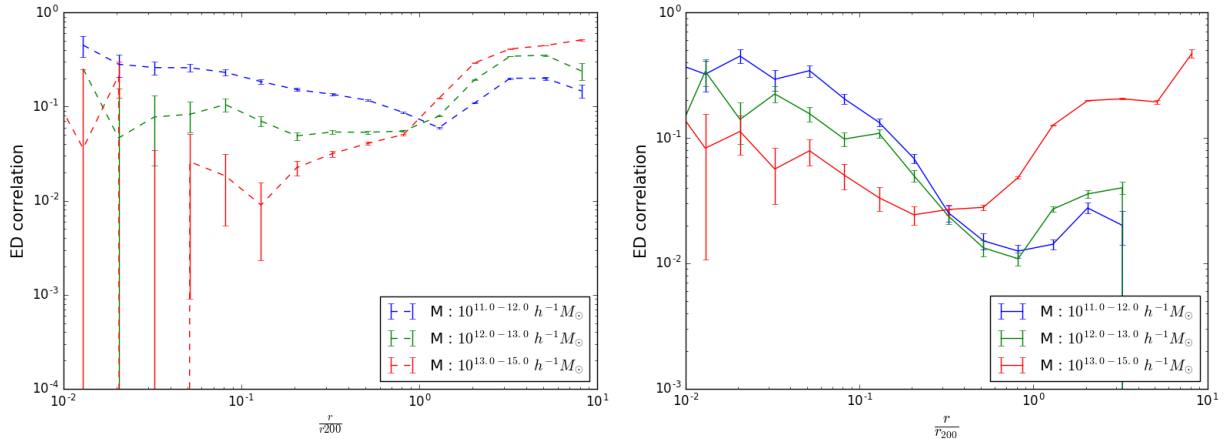


Figure 6. Ellipticity-direction (ED) correlation function of the 3D shape of the central galaxy with the location of the satellite galaxies within the given halo in MassiveBlack-II (*Left*) and Illustris-TNG (*Right*) simulations where the radial binning is in $\frac{r}{r_{200}}$. The correlation functions are plotted in halos of mass bins, $10^{11-12}h^{-1}M_{\odot}$, $10^{12-13}h^{-1}M_{\odot}$ and $10^{13-15}h^{-1}M_{\odot}$ at redshift, $z = 0.06$.

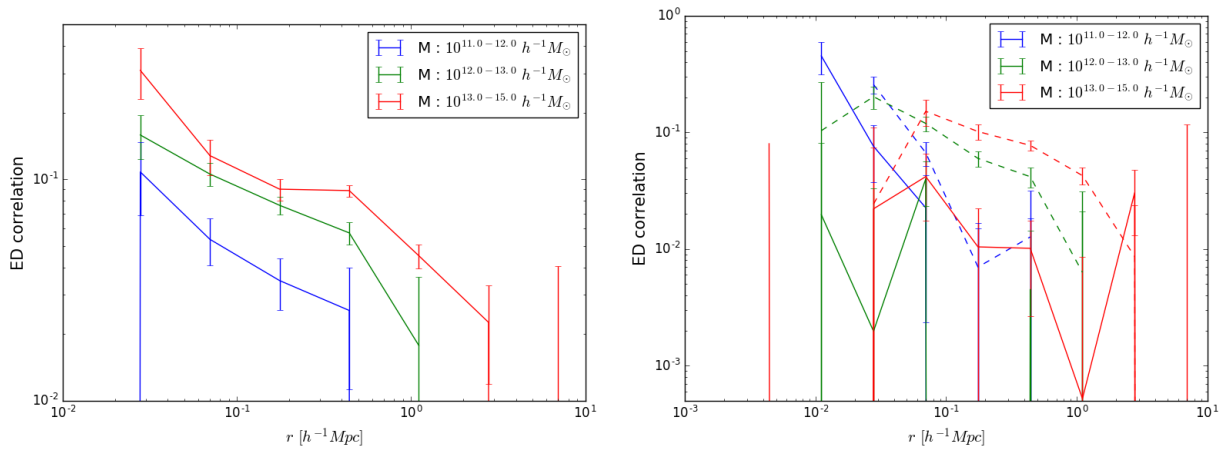


Figure 7. Ellipticity-direction (ED) correlation function of the 3D shape of the satellite galaxies with the location of the central galaxy within the given halo in MassiveBlack-II (*Left*) and Illustris-TNG (*Right*) simulations. The correlation functions are plotted in halos of mass bins, $10^{11-12}h^{-1}M_{\odot}$, $10^{12-13}h^{-1}M_{\odot}$ and $10^{13-15}h^{-1}M_{\odot}$ at redshift, $z = 0.06$. The dashed lines in the *Right* panel of the plot show the correlation function in Illustris simulation. (Note that we do not refer to the Illustris-TNG simulation here.)

component of the projected ellipticity, $\langle \epsilon_+ \rangle$ in Figure 8. The radial component of the ellipticity is calculated by

$$\epsilon_+ = \frac{1-q}{1+q} \cos[2\theta] \quad (6)$$

where, θ is the orientation of the major axis of the shape of satellite galaxy with respect to the halo center.

In Figure 8, we plot the mean radial ellipticity in halos of different mass bins. In both IllustrisTNG and MB-II simulations, we do not find a significant mass dependent trend in our measurements. While the satellite alignments in 3D show a radial dependence in the MassiveBlack-II simulation, the radial dependence is diluted in the alignment of the projected shapes with respect to the central galaxy. We further discuss the effects of projected shapes and projected distances on the radial alignment signal in Appendix A. However, the amplitude of the signal is roughly of the same order

of magnitude as the observational measurements⁴. It is to be noted that an exact comparison with observational measurements is difficult due to differences in shape measurement methods adopted and selection effects in observational data.

We also compare the radial dependence of the projected ellipticity component of the central galaxy with respect to the location of the satellite galaxies in Figure 9. The observational measurements found a decreasing trend with the radial distance. In MassiveBlack-II simulation, we notice a decreasing trend only in the lowest mass bin, $10^{11-12}h^{-1}M_{\odot}$. The radial dependence is not significant in the halo mass bin, $10^{12-13}h^{-1}M_{\odot}$, while the highest mass bin exhibits an in-

⁴ We note that there are no significant quantitative differences in the results when adopting the alternative definition for the ellipticity, $\epsilon = (1/2R)[(1-q^2)/(1+q^2)]$, where $R = 1 - e_{\text{rms}}^2$ is the shear responsivity factor, with e_{rms} being the rms ellipticity per component of the galaxy shape sample

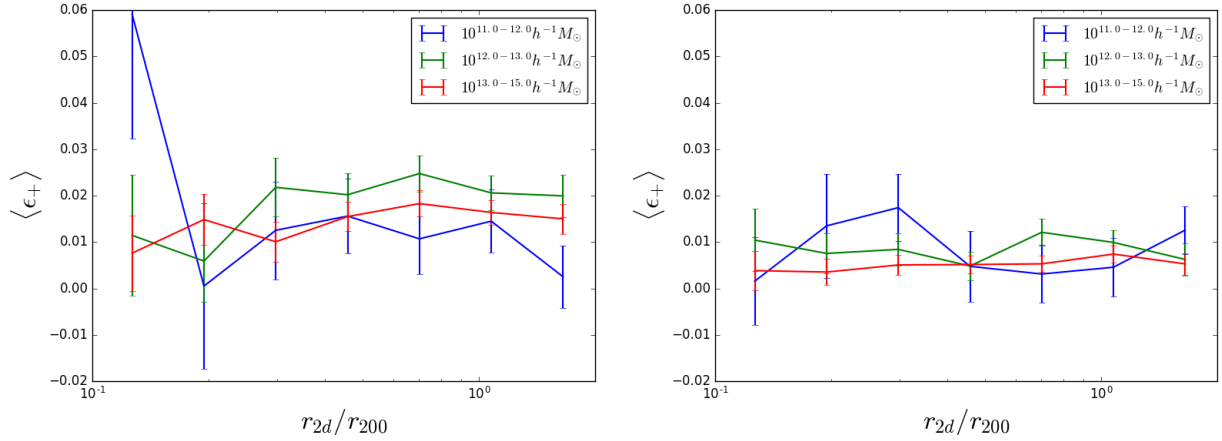


Figure 8. The mean of the radial component of the projected ellipticities of the shapes of the stellar component of the satellite galaxies with respect to the host central galaxy. Here, the binning is in $\frac{r_{2d}}{r_{200}}$, the ratio of the projected distance of the satellite to the central galaxy, r_{2d} and the r_{200} of the central galaxy. The mean radial ellipticities are shown for the MassiveBlack-II (*Left*) and Illustris-TNG (*Right*) simulations in halo mass bins of $10^{11-12} h^{-1} M_\odot$, $10^{12-13} h^{-1} M_\odot$ and $10^{13-15} h^{-1} M_\odot$.

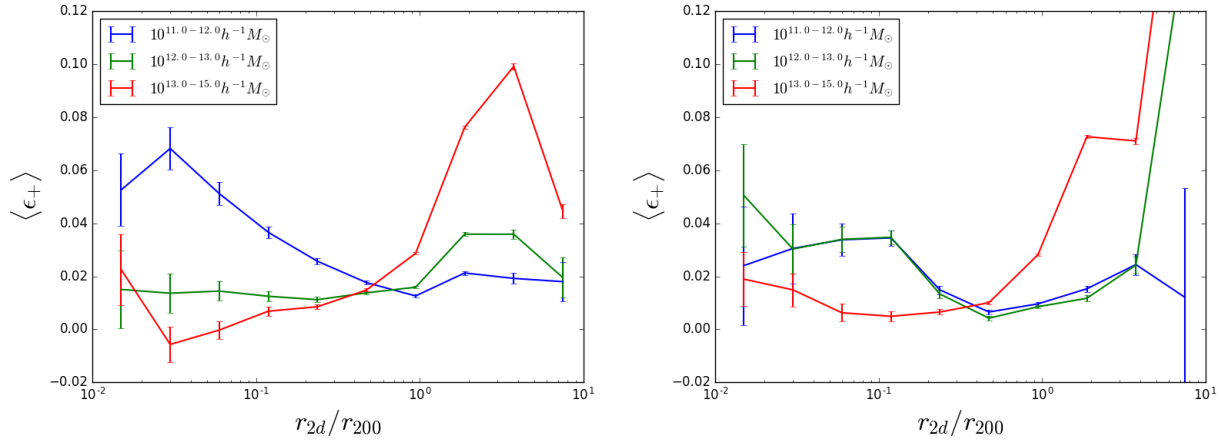


Figure 9. Mean radial ellipticity of the projected shape of the central galaxy with the location of the satellite galaxies within the given halo in MassiveBlack-II (*Left*) and Illustris-TNG (*Right*) simulations. Here, the binning is in $\frac{r_{2d}}{r_{200}}$, the ratio of the projected distance of the satellite to the central galaxy, r_{2d} and the r_{200} of the central galaxy. The mean ellipticities are plotted in halos of mass bins, $10^{11-12} h^{-1} M_\odot$, $10^{12-13} h^{-1} M_\odot$ and $10^{13-15} h^{-1} M_\odot$ at redshift, $z = 0.06$.

crease in the mean projected ellipticity with distance from center. This can be compared with the radial dependence trend for the 3D shapes shown in Figure 4. Similar to the ED correlation function in Figure 4, the mean ellipticity for the highest mass bin increases at large scales due to the anisotropic distribution of the satellites along the major axis of the dark matter shape. For the lower mass bins, the signal at large scales is diluted due to projection effects. We find a similar dependence in the Illustris-TNG simulation results shown in the right panel. The small-scale correlation functions in the larger volume Illustris-TNG 300 simulation and a detailed comparison of the different correlation functions in MassiveBlack-II, Illustris-TNG and Illustris-TNG300 simulations within the same halo mass bins is discussed in Appendix C. We find that the mass and radial dependent trend of the correlation functions is similar across all the simulations. However, the amplitude of alignment is larger in MassiveBlack-II.

4 CONCLUSIONS

In this paper, we study the anisotropic distribution of satellite galaxies along the orientation of the major axis of the stellar component of the central galaxy in MassiveBlack-II (Khandai et al. 2015) and IllustrisTNG (Nelson et al. 2019) simulations. The mitigation of intrinsic alignments in upcoming surveys such as LSST, *Euclid* and *WFIRST* requires a small-scale modelling of the galaxy alignments. Currently, halo model approaches for intrinsic alignments (Schneider & Bridle 2010) assume that the satellite galaxies are distributed spherically symmetric around the central galaxy and their orientation is pointed towards the location of central galaxy. We explore the deviations of galaxy alignments from the assumptions of halo model in realistic simulations of galaxy formation. We also compare our results with the measurements from observations and findings in other com-

parable simulations such as the EAGLE (Schaye et al. 2015) and Horizon-AGN (Dubois et al. 2014).

We first explore the alignment of the central galaxy shape with the shape of the satellite system traced by the positions of the satellite galaxies within the halo. In halos of mass greater than $10^{13} h^{-1} M_{\odot}$ at $z = 0.06$, we find that the satellite system is well aligned with the shape of central galaxy when compared to a random spherically symmetric distribution. This indicates that the satellites are distributed anisotropically along the major axis of the central galaxy, instead of a symmetric distribution. This is consistent with the findings in EAGLE simulation by Shao et al. (2016). Welker et al. (2015) also found similar alignment between the orientations of the minor axes of the galaxy in Horizon-AGN. We compared the distribution of satellite galaxies along the major axis of the central galaxy based on properties such as halo mass, luminosity, morphology, color and star formation rate. We found that the satellites tend to be more strongly distributed along the major axis in galaxies of larger halo mass. This trend is similar in both MassiveBlack-II and IllustrisTNG simulations. Similarly, the distribution of satellites is stronger in galaxies with higher luminosity. We also find that the satellite distribution is more anisotropic around central galaxies of lower star formation rate, spheroid morphology and red centrals.

We also explored the radial dependence of the satellite distribution and orientation of the satellite galaxy with the respect to the orientation and location respectively, of the major axis of the central galaxy of the host halo. Looking at the radial alignments in 3D, we find that at small scales, the satellites are distributed along the major axis of the central galaxy and the correlation decreases as the distance from the central galaxy increases. However at distances reaching the boundary of the halo, we find that the correlation increases. This is due to the satellites on the outer regions of the halo being more anisotropically distributed along the orientation of the shape of the dark matter component of the galaxy, which is correlated with the shape of the stellar component.

We studied the radial dependence of the shape of the satellite galaxies with respect to the location of central galaxy. in MassiveBlack-II, we find that the galaxies at smaller distances from the central tend to point more strongly towards the location of central galaxy. The correlation decreases as distance from the center increases. We also find a similar trend in the Illustris simulation. However, we do not find a significant radial trend of satellite orientation in the IllustrisTNG simulation. The different trends in Illustris and IllustrisTNG simulation points to the effects of variations in baryonic feedback on satellite galaxy alignments. Finally, we compared the simulation measurements of projected correlation functions on small scales with the observational measurements from the GAMA+KiDS galaxies Georgiou et al. (2019). From observations, Georgiou et al. (2019) found a radially decreasing trend of the satellite ellipticity with respect to the location of central galaxy. However, in MassiveBlack-II and IllustrisTNG, we do not find a radial trend in the mean satellite ellipticity. However, the amplitude of the mean radial ellipticity is consistent with the observational measurements. We note that the projection effects decreases the radial dependence of the satellite alignments in simulations and leads to a scale-independent radial trend.

The results from this study should help to inform the halo model approaches to model galaxy alignments on small scales. In future work, we plan to incorporate mock galaxy alignments in Euclid Flagship simulation (Potter et al. 2017), taking into account the mass and radial dependence of satellite alignments in hydrodynamic simulations.

ACKNOWLEDGMENTS

AT acknowledges funding from Enabling Weak lensing Cosmology (EWC) through European Unions Horizon 2020 research and innovation programme under grant agreement No 776247. TK is supported by a Royal Society University Research Fellowship and EWC. AT thanks Rachel Mandelbaum and Henk Hoekstra for feedback on this work. TDM acknowledges funding from NSF ACI-1614853, NSF AST-1517593, NSF AST-1616168 and NASA ATP 19-ATP19-0084. TDM also acknowledges funding from NASA ATP 80NSSC18K101, and NASA ATP NNX17AK56G.

REFERENCES

- Blazek J., Mandelbaum R., Seljak U., Nakajima R., 2012, *JCAP*, **2012**, 041
- Blazek J., Vlah Z., Seljak U., 2015, *Journal of Cosmology and Astroparticle Physics*, 2015, 015
- Bridle S., King L., 2007, *New Journal of Physics*, **9**, 444
- Catelan P., Kamionkowski M., Blandford R. D., 2001, *Monthly Notices of the Royal Astronomical Society*, **320**, L7
- Chisari N., et al., 2015, *MNRAS*, **454**, 2736
- Di Matteo T., Khandai N., DeGraf C., Feng Y., Croft R. A. C., Lopez J., Springel V., 2012, *ApJ*, **745**, L29
- Dubois Y., et al., 2014, *MNRAS*, **444**, 1453
- Genel S., et al., 2014, *MNRAS*, **445**, 175
- Georgiou C., et al., 2019, arXiv e-prints, p. [arXiv:1905.00370](#)
- Hilbert S., Xu D., Schneider P., Springel V., Vogelsberger M., Hernquist L., 2017, *MNRAS*, **468**, 790
- Hirata C. M., Seljak U. c. v., 2004, *Phys. Rev. D*, **70**, 063526
- Huang H.-J., Mandelbaum R., Freeman P. E., Chen Y.-C., Rozo E., Rykoff E., Baxter E. J., 2016, *MNRAS*, **463**, 222
- Huang H.-J., Mandelbaum R., Freeman P. E., Chen Y.-C., Rozo E., Rykoff E., 2018, *MNRAS*, **474**, 4772
- Joachim B., Bridle S. L., 2010, *A&A*, **523**, A1
- Katz N., Weinberg D. H., Hernquist L., 1996, *ApJS*, **105**, 19
- Khandai N., Di Matteo T., Croft R., Wilkins S., Feng Y., Tucker E., DeGraf C., Liu M.-S., 2015, *MNRAS*, **450**, 1349
- Kirk D., Rassat A., Host O., Bridle S., 2012, *MNRAS*, **424**, 1647
- Komatsu E., et al., 2011, *ApJS*, **192**, 18
- Krause E., Eifler T., Blazek J., 2016, *MNRAS*, **456**, 207
- LSST Science Collaboration et al., 2009, arXiv e-prints, p. [arXiv:0912.0201](#)
- Laureijs R., et al., 2011, arXiv e-prints, p. [arXiv:1110.3193](#)
- Marinacci F., et al., 2018, *MNRAS*, **480**, 5113
- Naiman J. P., et al., 2018, *MNRAS*, **477**, 1206
- Nelson D., et al., 2018, *MNRAS*, **475**, 624
- Nelson D., et al., 2019, *Computational Astrophysics and Cosmology*, **6**, 2
- Pillepich A., et al., 2018a, *MNRAS*, **473**, 4077
- Pillepich A., et al., 2018b, *MNRAS*, **475**, 648
- Planck Collaboration et al., 2016, *A&A*, **594**, A13
- Potter D., Stadel J., Teyssier R., 2017, *Computational Astrophysics and Cosmology*, **4**, 2
- Samuroff S., Mandelbaum R., Di Matteo T., 2019, arXiv e-prints, p. [arXiv:1901.09925](#)
- Schaye J., et al., 2015, *MNRAS*, **446**, 521

- Schneider M. D., Bridle S., 2010, *Monthly Notices of the Royal Astronomical Society*, 402, 2127
- Shao S., Cautun M., Frenk C. S., Gao L., Crain R. A., Schaller M., Schaye J., Theuns T., 2016, *MNRAS*, 460, 3772
- Soussana A., et al., 2019, arXiv e-prints, p. arXiv:1908.11665
- Spergel D., et al., 2015, arXiv e-prints, p. arXiv:1503.03757
- Springel V., 2010, *MNRAS*, 401, 791
- Springel V., Hernquist L., 2003, *MNRAS*, 339, 289
- Springel V., Di Matteo T., Hernquist L., 2005, *MNRAS*, 361, 776
- Springel V., et al., 2018, *MNRAS*, 475, 676
- Tenneti A., Singh S., Mandelbaum R., di Matteo T., Feng Y., Khandai N., 2015, *MNRAS*, 448, 3522
- Tenneti A., Mandelbaum R., Di Matteo T., 2016, *MNRAS*, 462, 2668
- Tenneti A., Gnedin N. Y., Feng Y., 2017, *ApJ*, 834, 169
- Velliscig M., et al., 2015, *MNRAS*, 454, 3328
- Vogelsberger M., et al., 2014a, *MNRAS*, 444, 1518
- Vogelsberger M., et al., 2014b, *Nature*, 509, 177
- Weinberger R., et al., 2017, *MNRAS*, 465, 3291
- Welker C., Dubois Y., Pichon C., Devriendt J., Chisari E. N., 2015, arXiv e-prints, p. arXiv:1512.00400
- van Uitert E., et al., 2017, *MNRAS*, 467, 4131

APPENDIX A: PROJECTION EFFECTS ON SATELLITE SHAPE - CENTRAL POSITION CORRELATION FUNCTIONS

Here, we explore the effects of projected shapes and projected distances on the radial dependence of satellite alignments in more detail. In the left panel of Figure A1, we plot the ED correlation of the 3D stellar shapes and projected (2D) shapes of the satellite galaxies with the location of the central galaxies as a function of the 3D distance. We can observe a slight decrease in the amplitude of alignment when using projected shapes. However, the radial scaling is similar to 3D shapes. In the right panel of Figure A1, we plot the alignment of the projected shapes, but the distances are binned in 3D and 2D. When binned in 2D distances, we can observe a loss of radial dependence in the satellite alignment. In Figure A2, we plot the mean radial ellipticities of the projected shapes with distances binned in r_{3d}/r_{200} in MassiveBlack-II and IllustrisTNG simulations. In MassiveBlack-II, the decreasing radial dependence of the signal is seen in the highest mass bin, and weakly in the lower mass bins too. The TNG simulations show a radial dependence in the lower mass bins, but not in the highest mass bin which is also the case in 3D satellite alignments as discussed before in Section 3.3. So, we can conclude that the lack of radial dependence in the mean projected ellipticities of the satellite galaxies in simulations is mainly due to the effects of binning in projected distances and to some extent due to normalization with r_{200} . The projected satellite shapes still tend to point towards the central galaxies with a stronger alignment at smaller distances.

APPENDIX B: ED CORRELATION FUNCTIONS OF CENTRALS WITH SATELLITES WITHIN R_{200}

In Figure B1, we plot the ED correlation function of the central galaxy shape with position of satellite galaxies, including satellites only within the distance of r_{200} for the given

halo in the density sample. This is to understand if the increasing trend of the correlation function on large scales is seen when only satellite galaxies within r_{200} are considered. For the highest mass bin, we can clearly see that the trend is similar to what we find using all satellites within the halo. This is consistent with our earlier discussion in Section 3.3 that the increase in correlation is due to the satellites on outer regions of halo tracing the shape of the dark matter halo.

APPENDIX C: SMALL-SCALE CORRELATION FUNCTIONS IN ILLUSTRIS-TNG300 SIMULATION

Here, we also extend the small-scale correlation functions to the larger volume Illustris-TNG300 simulation of boxsize $205h^{-1}\text{Mpc}$ at $z = 0.06$. In Figure C1, we plot the ED correlation function of the the alignment of the shape of the central galaxies with the location of satellites (*Left* panel) and also the satellite alignment with central galaxy position (*Right* panel) in the halo mass bins $10^{11-12}h^{-1}M_{\odot}$, $10^{12-13}h^{-1}M_{\odot}$ and $10^{13-15}h^{-1}M_{\odot}$. Figure C2 shows the projected mean ellipticities of the central shapes and satellite shapes with respect to the position of satellite and central galaxies respectively. In general, the mass dependent trend of all the correlations function is similar to those of Massive-Black II and TNG100 simulations discussed in Section 3.3. However, for the alignments of the 3D shapes of satellite galaxies with respect to the central (*Right* panel of Figure C1), we find a radially decreasing correlation function only in the highest mass bin. This is possibly due to fewer satellites in the lowest mass bin of TNG300 simulation, as the resolution is smaller when compared with TNG100. In Figures C3, C4, C5 and C6, we compare the alignment signals of the small-scale correlation functions in TNG300 simulation with those of TNG and Massive-Black II results within the same halo mass bins. Based on the ED correlation functions of the central galaxy shape with the satellite position shown in Figure C3, we can see that the amplitude of correlation function is higher for the central galaxies in TNG300 simulation, when compared to the galaxies in TNG100 in all mass bins while the radial scaling is similar. It is likely that the smaller resolution in the TNG300 simulation, box-size effects can lead to different galaxy properties and alignments although the baryonic physics model is the same. We have separately verified that the disk galaxy fraction is smaller in TNG300 simulation at all masses and the change in morphological fraction can be one of the reasons for stronger alignments in TNG300. The correlation function in Massive-Black II have larger amplitudes in the two lower mass bins, while the amplitude is similar in the highest mass bin. As discussed in Section 3.1, the satellite anisotropy is larger in MassiveBlack-II due to the stronger alignment of the shape of the stellar component with that of the dark matter component. Comparing the 3D satellite alignments in Figure C4, the amplitude of alignments are larger in the Massive-Black II simulation for all mass bins. In the TNG300 simulation, we can observe a significant satellite alignment signal only in the highest mass bin, where the alignment is higher than TNG100. The lack of resolution leads to no sufficient number of satellites in the lowest

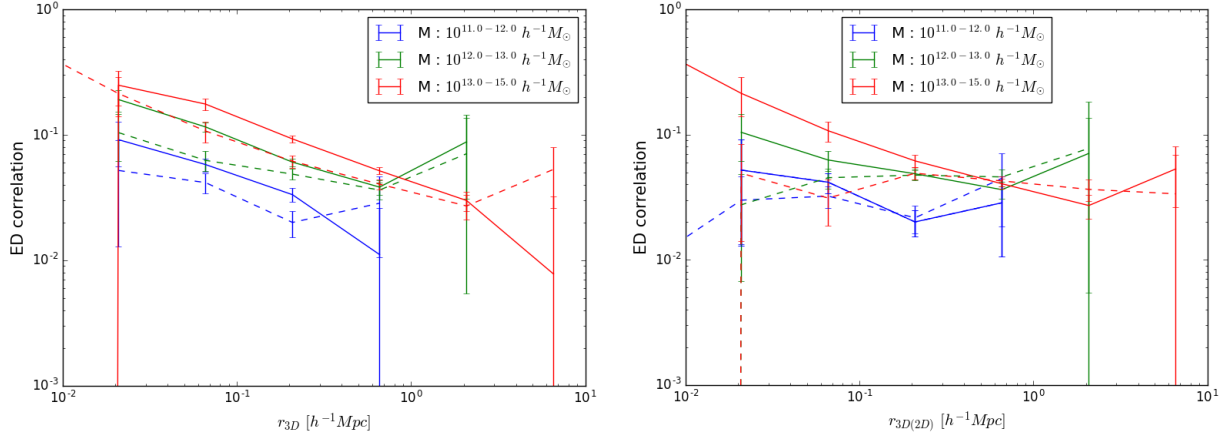


Figure A1. *Left:* Ellipticity-direction (ED) correlation function of the 3D and 2D (projected) shape of the satellite galaxies with the location of the central galaxy within the given halo. *Right:* ED correlation of 2D shape of satellite galaxies with distances measured in 3D and 2D. The correlation functions are plotted in halos of mass bins, $10^{11-12}h^{-1}M_{\odot}$, $10^{12-13}h^{-1}M_{\odot}$ and $10^{13-15}h^{-1}M_{\odot}$ at redshift, $z = 0.06$.

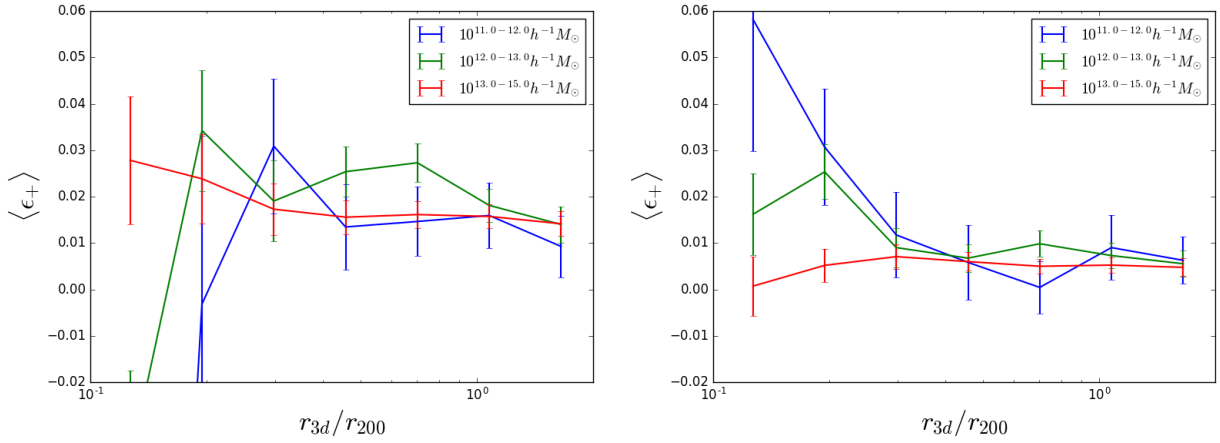


Figure A2. The mean of the radial component of the projected ellipticities of the shapes of the stellar component of the satellite galaxies with respect to the host central galaxy. Here, the binning is in $\frac{r_{3d}}{r_{200}}$, the ratio of the 3D distance of the satellite to the central galaxy, r_{3d} and the r_{200} of the central galaxy. The mean radial ellipticities are shown for the MassiveBlack-II (*Left*) and Illustris-TNG (*Right*) simulations in halo mass bins of $10^{11-12}h^{-1}M_{\odot}$, $10^{12-13}h^{-1}M_{\odot}$ and $10^{13-15}h^{-1}M_{\odot}$.

mass bins. The mean projected ellipticities of the satellite shapes with central positions are compared in Figure C5. Similar to satellite alignments in 3D, the amplitude of mean projected ellipticities are larger in Massive-Black II. Similar to Massive-Black II, we do not observe a radial dependence of the projected satellite alignment in both TNG100 and TNG300 simulations. As seen from Figure C6, the projected ellipticities of the central galaxies are similar in the lowest and highest halo mass bins. The correlation functions for Massive-Black II galaxies in the intermediate mass bin shows a smaller amplitude on small scales, but higher on large scales when compared to those of TNG simulations.

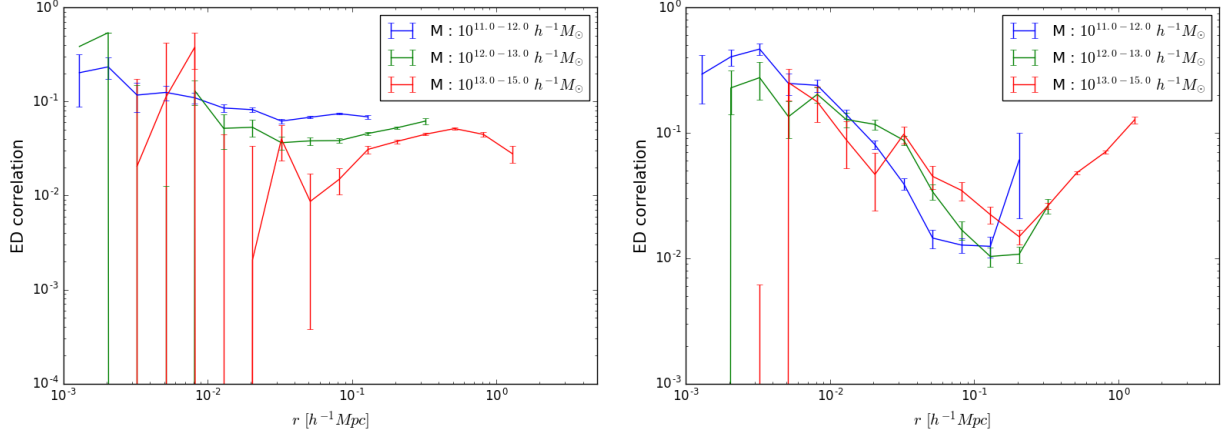


Figure B1. Ellipticity-direction (ED) correlation function of the 3D shape of the central galaxy with the location of the satellite galaxies within the distance, r_{200} of the given halo in MassiveBlack-II (*Left*) and Illustris-TNG (*Right*) simulations. The correlation functions are plotted in halos of mass bins, $10^{11-12} h^{-1} M_{\odot}$, $10^{12-13} h^{-1} M_{\odot}$ and $10^{13-15} h^{-1} M_{\odot}$ at redshift, $z = 0.06$.

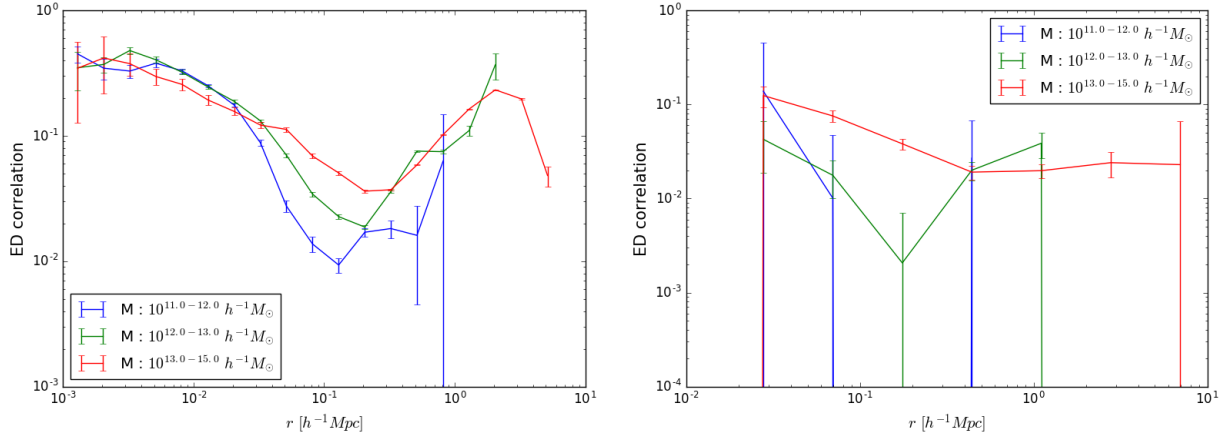


Figure C1. *Left:* Ellipticity-direction (ED) correlation function of the 3D shape of the central galaxy with the location of the satellite galaxies within the given halo in Illustris-TNG300 simulation(*Left*). *Right:* Ellipticity-direction (ED) correlation function of the 3D shape of the satellite galaxies with the location of the central galaxy within the given halo. The correlation functions are plotted in halos of mass bins, $10^{11-12} h^{-1} M_{\odot}$, $10^{12-13} h^{-1} M_{\odot}$ and $10^{13-15} h^{-1} M_{\odot}$ at redshift, $z = 0.06$.

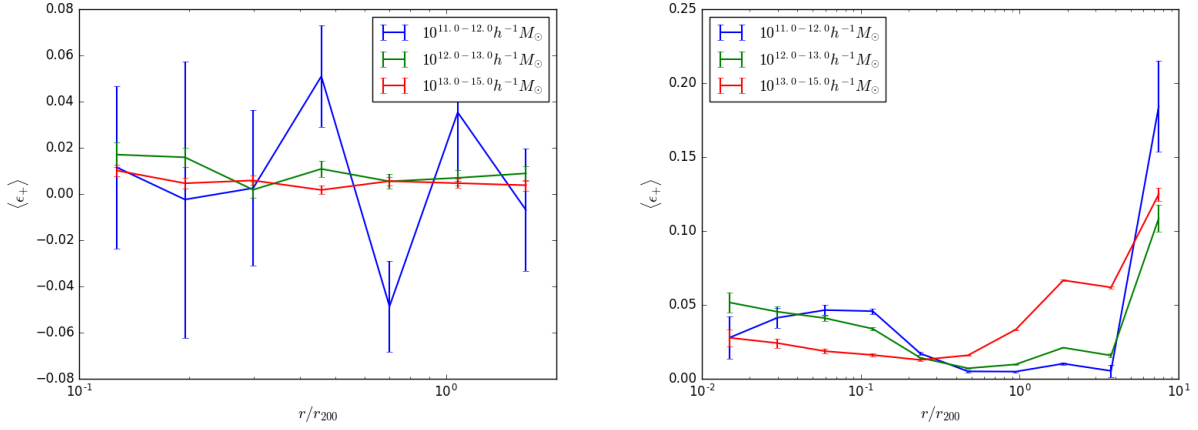


Figure C2. *Left:* The mean of the radial component of the projected ellipticities of the shapes of the stellar component of the satellite galaxies with respect to the host central galaxy. The mean radial ellipticities are shown for the Illustris-TNG300 simulation in halo mass bins of $10^{11-12} h^{-1} M_{\odot}$, $10^{12-13} h^{-1} M_{\odot}$ and $10^{13-15} h^{-1} M_{\odot}$. *Right:* Mean radial ellipticity of the projected shape of the central galaxy with the location of the satellite galaxies within the given halo.

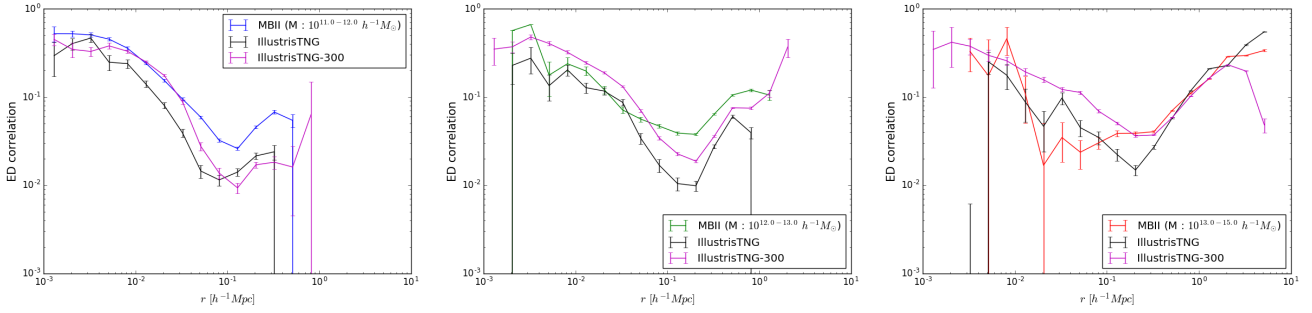


Figure C3. *Left:* The mean of the radial component of the projected ellipticities of the shapes of the stellar component of the satellite galaxies with respect to the host central galaxy. The mean radial ellipticities are shown for the Illustris-TNG300 simulation in halo mass bins of $10^{11-12} h^{-1} M_{\odot}$, $10^{12-13} h^{-1} M_{\odot}$ and $10^{13-15} h^{-1} M_{\odot}$. *Right:* Mean radial ellipticity of the projected shape of the central galaxy with the location of the satellite galaxies within the given halo.

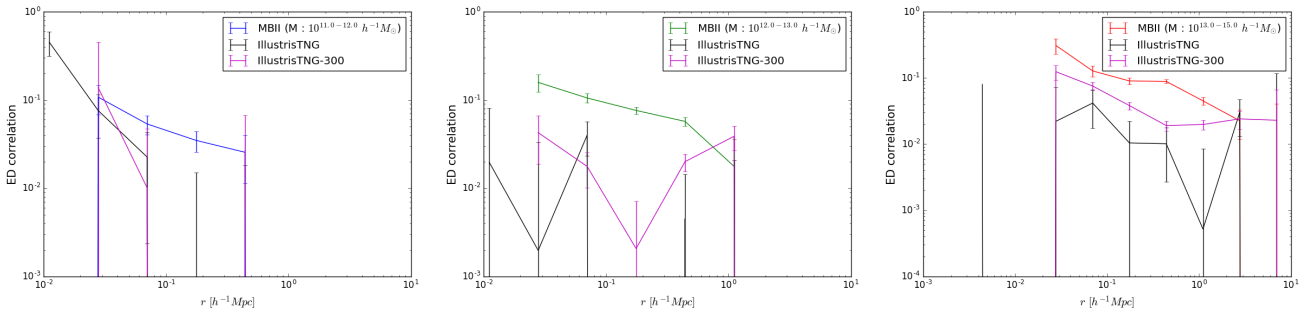


Figure C4. *Left:* Ellipticity-direction (ED) correlation function of the 3D shape of the central galaxy with the location of the satellite galaxies within the given halo in Illustris-TNG300 simulation (Left). *Right:* Ellipticity-direction (ED) correlation function of the 3D shape of the satellite galaxies with the location of the central galaxy within the given halo. The correlation functions are plotted in halos of mass bins, $10^{11-12} h^{-1} M_{\odot}$, $10^{12-13} h^{-1} M_{\odot}$ and $10^{13-15} h^{-1} M_{\odot}$ at redshift, $z = 0.06$.

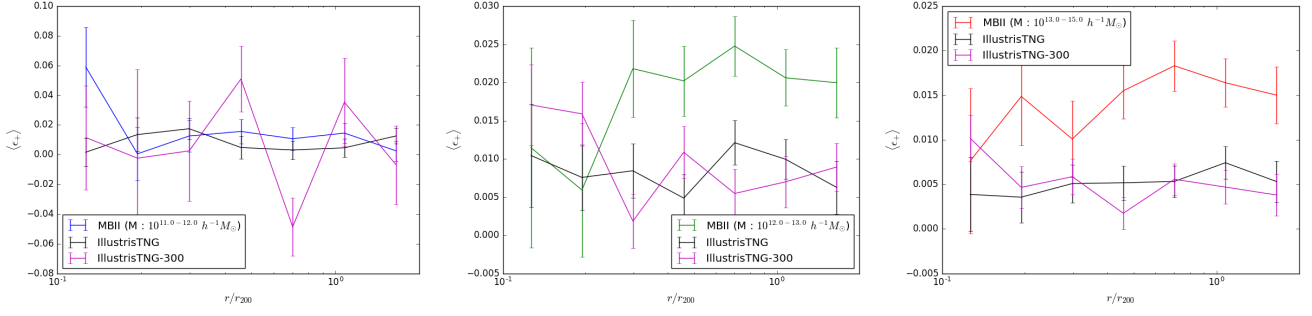


Figure C5. *Left:* The mean of the radial component of the projected ellipticities of the shapes of the stellar component of the satellite galaxies with respect to the host central galaxy. The mean radial ellipticities are shown for the Illustris-TNG300 simulation in halo mass bins of $10^{11-12} h^{-1} M_\odot$, $10^{12-13} h^{-1} M_\odot$ and $10^{13-15} h^{-1} M_\odot$. *Right:* Mean radial ellipticity of the projected shape of the central galaxy with the location of the satellite galaxies within the given halo.

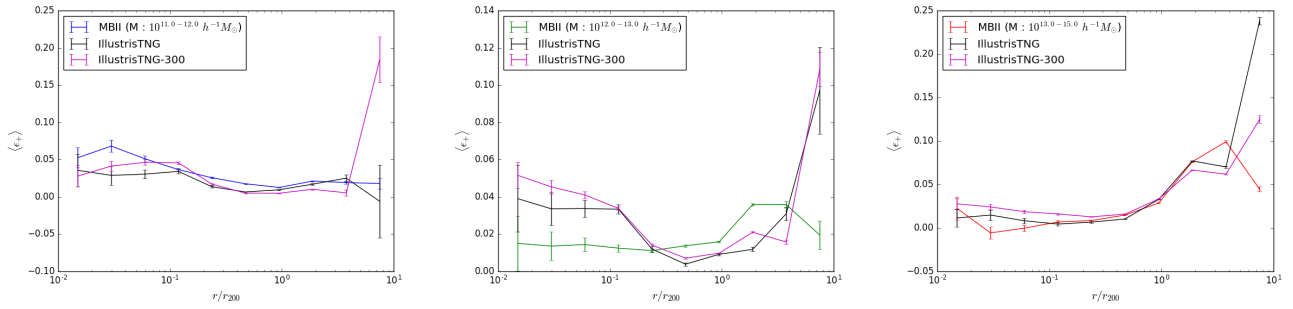


Figure C6. *Left:* Ellipticity-direction (ED) correlation function of the 3D shape of the central galaxy with the location of the satellite galaxies within the given halo in Illustris-TNG300 simulation. *Right:* Ellipticity-direction (ED) correlation function of the 3D shape of the satellite galaxies with the location of the central galaxy within the given halo. The correlation functions are plotted in halos of mass bins, $10^{11-12} h^{-1} M_\odot$, $10^{12-13} h^{-1} M_\odot$ and $10^{13-15} h^{-1} M_\odot$ at redshift, $z = 0.06$.